Squeeze dispersion: modulation of diapycnal mixing by diapycnal strain

Gregory L Wagner[1], Glenn Flierl[1], Raffaele Ferrari[1], Gunnar Voet[2], Glenn S Carter[3], Matthew H Alford[2], and James B Girton[4]

[1]Earth, Atmospheric, and Planetary Sciences, Massachusetts Institute of Technology, Cambridge, MA 02139
[2]Scripps Institution of Oceanography, La Jolla, CA 90237
[3]Department of Oceanography, University of Hawai'i at Manoa, Honolulu, HI 96822
[4]Applied Physics Laboratory, University of Washington, Seattle, Washington

Key Points:

- Squeezing and stretching density layers modulates the diapycnal diffusion of oceanic tracers
- Squeeze dispersion enhances dispersion by 2–3x across some isopycnals in the abyssal Samoan Passage
- Diapycnal transport is strongly affected by positive correlations between squeezing and turbulence

Corresponding author: Gregory L Wagner, `wagner.greg@gmail.com`

Abstract

We describe a process called 'squeeze dispersion' in which the squeezing of isopycnal surfaces by waves, eddies, and bathymetric flow modulates the diapycnal diffusion of oceanic tracers by centimeter to meter-scale turbulence. Squeeze dispersion typically enhances diffusion — especially when diffusivity positively correlates with squeezing. We introduce squeeze dispersion with an idealized example, and derive an equation for the circulation of oceanic tracers that establishes the fundamental role of squeeze dispersion and its associated effective diffusivity in oceanic diapycnal mixing. We use the squeeze dispersion effective diffusivity to interpret observations of abyssal flow through the Samoan Passage reported by Alford et al. (2013) and find that correlations between squeezing and turbulent diffusivity enhance tracer dispersion across some isopycnals by factors of 2–3.

Plain language summary

Vertical ocean mixing, which is weak and mediates Earth's climate by drawing atmospheric carbon and heat in the deep ocean, depends on turbulence that churns the ocean on the tiny scales of centimeters to meters. We demonstrate that vertical ocean mixing depends not *only* on this small scale turbulence as previously thought, but on the *correlation* between small scale turbulence and larger-scale motions like currents and eddies on horizontal scales of ten to hundreds of kilometers — the oceanic versions of jet streams and hurricanes. In particular, when a patch of ocean is mixed by small-scale turbulence while being 'squeezed' in the vertical at the same time by currents and eddies, the patch ultimately mixes more quickly than the turbulence would cause alone. This means that we need to know something both about about typical rates of oceanic squeezing as well as typical oceanic small-scale turbulence to estimate the total rate of oceanic vertical mixing.

1 Introduction

Squeeze dispersion is a process in which the diapycnal diffusion of oceanic tracers such as dissolved carbon, temperature, salinity, density, oxygen, nutrients, or plankton is modulated in fluctuating flows that alternately squeeze isopycnal surfaces together and stretch them apart. In general, squeeze dispersion is important in flows with significant strain but negligible net transport in one or more directions. Such flows may occur under strong geometric or dynamical constraints: for example, low Reynolds flows confined by solid boundaries, or stratified, rotating, and anisotropic planetary flows. We focus on oceanic flows, where squeeze dispersion associated with waves, eddies, and bathymetric flow modifies the diapycnal dispersion of circulating oceanic tracers.

A parameterization for the diffusive flux between two fluctuating fluid surfaces illustrates the basic mechanism of squeeze dispersion. Consider the scenario sketched in figure 1, in which a material surface with tracer concentration c_2 overlies a material surface with concentration c_1. The vertical diffusive tracer flux between the two layers is $F = -\kappa(c_2 - c_1)/h$, where h is the vertical separation between the surfaces. The tracer flux averaged over fluctuations in both h and κ is $\langle F \rangle = -(c_2 - c_1) \langle \kappa/h \rangle$. To express $\langle F \rangle$ in terms of the average separation between the surfaces $\langle h \rangle$ we introduce the effective squeeze dispersion diffusivity,

$$\kappa_s = \langle h \rangle \left\langle \frac{\kappa}{h} \right\rangle , \tag{1}$$

such that $\langle F \rangle = -\kappa_s (c_2 - c_1)/\langle h \rangle$. Because $\langle 1/h \rangle \geq 1/\langle h \rangle$, equation (1) implies that fluctuations in h always enhance the effective diffusivity κ_s over cases with constant h when κ is constant. When squeezing (small h), and elevated microstructure turbulence (large κ) are correlated — a scenario encountered in Samoan Passage observations analyzed in section 4 — the enhancement of diffusion due to squeeze dispersion is greater still.

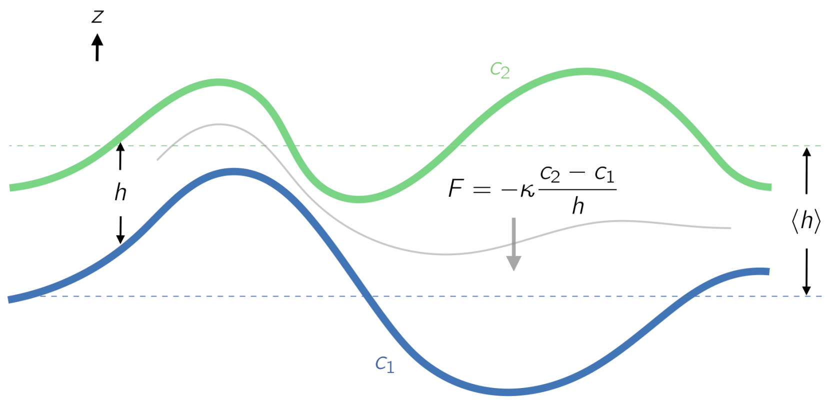

Figure 1: Illustration of squeeze dispersion between two isotracer surfaces with tracer concentrations c_2 and c_1. The diffusive flux between the fluctuating surfaces is $F = -\kappa \left(c_2 - c_1\right)/h$, where h is the separation between the surfaces and κ is diffusivity. The spatially-averaged separation between the two surfaces is $\langle h \rangle$. Introducing an effective squeeze dispersion diffusivity $\kappa_s = \langle h \rangle \langle \kappa / h \rangle$ implies that $\langle F \rangle = -\left(c_2 - c_1\right) \kappa_s / \langle h \rangle$.

In section 2 we examine a concrete example of squeeze dispersion in the advection of a tracer patch over undulating bathymetry by a spatially-variable, squeezing and stretching barotropic flow. We then derive an equation that describes the dispersion of tracers on the scales of ocean circulation in section 3 in which diapycnal squeeze dispersion associated with submesoscale and mesoscale strain manifests alongside the familiar processes of advection by the residual-mean circulating velocity and isopycnal diffusive mixing by mesoscale eddies. This tracer circulation equation demonstrates the fundamental role that squeeze dispersion plays in ocean mixing.

We conclude with an analysis of observations that implies squeeze dispersion enhances the turbulent diffusion of tracers advected through the Samoan Passage across some isopycnals by factors of 2–3. In other words, we find that realistic variations in turbulent diffusivity and squeezing significantly alter the effective diffusivity of oceanic tracers. The difference between average diffusivity and effective squeeze dispersion diffusivity may contribute to differences between tracer-based and microstructure-based estimates of diapycnal diffusivity inferred from observations in the Brazil Basin (Ledwell et al., 2000), the east Pacific sector of the Antarctic Circumpolar Current (Ledwell, St. Laurent, Girton, & Toole, 2011), and Drake Passage (Mashayek et al., 2017; St. Laurent et al., 2012; Watson et al., 2013).

2 Squeeze dispersion in flow over undulating bathymetry

Oceanic squeeze dispersion is illustrated by the two-dimensional dispersion of a tracer patch advected by barotropic flow over undulating bathymetry. The advection of the tracer patch through the contracting streamlines of the bathymetric flow $u(x)$, $w(x, z)$ approximates the squeezing of oceanic tracer gradients between fluctuating isopycnal surfaces, while the effects of microstructure turbulent mixing are modeled by an inhomogeneous turbulent diffusivity, $\kappa(x, z, t)$. The concentration of tracer patch $c(x, z, t)$ obeys the advection-diffusion equation

$$c_t + u c_x + w c_z = \partial_x \left(\kappa c_x\right) + \partial_z \left(\kappa c_z\right) \,, \tag{2}$$

where $\kappa(x, z, t)$ is the diffusivity induced by turbulence on scales much smaller than the flow, and the barotropic horizontal and vertical velocity are

$$u(x) = \frac{U}{H} \qquad \text{and} \qquad w(x, z) = \frac{zUH_x}{H^2}\,, \tag{3}$$

with barotropic transport U, length L, depth

$$H(x) = \langle H \rangle \left[1 - \Delta \sin\left(\tfrac{2\pi x}{L}\right)\right]\,, \tag{4}$$

average depth $\langle H \rangle$, and non-dimensional relative bathymetric height Δ.

Figure 2(a) shows the evolution of an initially Gaussian tracer patch squeezed and stretched by the flow in (3) with constant κ. We compare the prescribed κ to the measured effective diffusivity $\kappa_s = (2T)^{-1} \int (Z - z)^2 c \,\mathrm{d}x\mathrm{d}z$, where $Z = \int zc \,\mathrm{d}x\mathrm{d}z$ is the z-centroid of the tracer patch, based on the change in the vertical variance of the tracer patch over the interval $T = \langle H \rangle L/U$ during which the patch travels from $x = 0$ to $x = L$. This definition of κ_s, introduced by Aris (1956), is used to interpret oceanic tracer release experiments such as that reported by Ledwell et al. (2011). The numerical results are plotted as blue circles in figure 2(b), showing that the measured effective diffusivity exceeds the prescribed constant diffusivity. This is squeeze dispersion: tracer dispersion increases with increasing Δ and thus increasing squeezing, despite acceleration of the tracer patch over the constriction and stretching over the contraction.

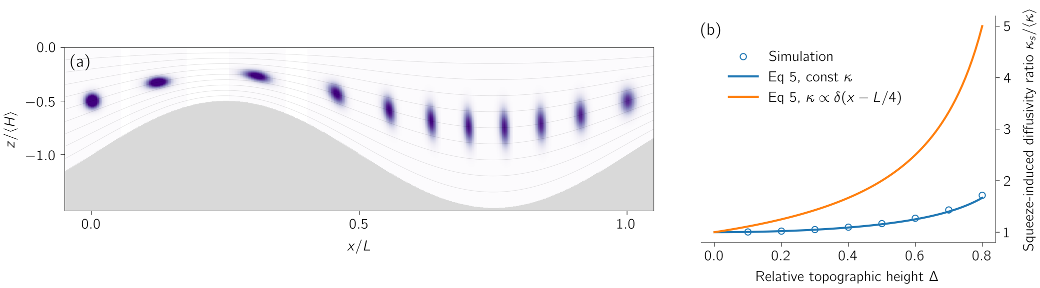

Figure 2: (a) Time-lapse of a tracer patch advected by the barotropic flow in (3) over a wavy bottom with relative bathymetric height $\Delta = 0.5$ at the 11 equispaced times $t = jT/10$ with $j = 0$–10 and $T = \langle H \rangle L/U$. (b) Enhancement of dispersion due to squeezing by the bathymetric flow in (3) in a numerical simulation of (2) (blue circles) and the approximate theoretical prediction 6 with constant κ (blue solid line) and a 'hot spot' with $\kappa \propto \delta(x - L/4)$ (orange solid line). We use $U = 1$, $\langle H \rangle = 1$, $L = 20$, $\kappa = 10^{-4}\,\mathrm{m^2\,s^{-1}}$ and tracer initial condition $c(t = 0) = \mathrm{e}^{-x^2/2\ell^2 - (z + \langle H \rangle/2)^2/2d^2}/2\pi\ell d$ with $\ell = L/100$ and $d = \langle H \rangle/20$.

The nature of this dispersion enhancement is revealed by a special solution to (2)–(3) derived in appendix A in which we assume the tracer patch has a thin aspect ratio such that $\partial_x(\kappa c_x) \ll \partial_z(\kappa c_z)$, use a transformation into bathymetric coordinates with the initial condition $c(t = 0) = \delta(x)\delta(z + \langle H \rangle/2)$, and allow turbulent diffusivities of the form $\kappa(x, t)$. The tracer distribution in this solution is tellingly Gaussian after being advected for a time $t_n = n\langle H \rangle L/U$ through n 'squeezing cycles' over the periodic bathymetry,

$$c(t = t_n) = \frac{1}{\sqrt{4\pi\kappa_s t_n}} \exp\left[-\frac{(z + \langle H \rangle/2)^2}{4\kappa_s t_n}\right] \delta(x - nL)\,, \tag{5}$$

and therefore spreads diffusively in the vertical while advected horizontally. However, rather than spreading with the trajectory-averaged diffusivity, for example, the effective diffusivity that determines tracer patch dispersion is

$$\kappa_s = \langle H \rangle \left\langle \frac{\kappa}{H} \right\rangle , \qquad \text{where} \qquad \langle \phi \rangle \stackrel{\text{def}}{=} \frac{1}{L} \int_0^L \phi \, \mathrm{d}x \, . \tag{6}$$

κ_s in (5)–(6) is identical to the effective diffusivity defined in terms of the growth of tracer variance, $\kappa_s = (2T)^{-1} \int (Z - z)^2 c \, \mathrm{d}x \mathrm{d}z$. Because $\langle 1/H \rangle \geq 1/\langle H \rangle$ for any positive function $H(x)$, (6) implies that fluctuating squeezing always enhances the diffusive transport associated with a constant κ. Moreover, the enhancement is increased further relative to $\langle \kappa \rangle$ when κ and squeezing positively correlate.

In figure 3(b) we compare the diffusivity enhancement $\kappa_s / \langle \kappa \rangle$ in numerical solutions to (2) (circles) with the theoretical prediction (6) (solid lines) versus Δ. The slight disagreement between the two solutions, which show that enhancement is relatively modest for constant κ, is due to the contribution of horizontal diffusion and shear to the vertical dispersion of the patch in the numerical solution. The orange solid line plots (6) for a diffusivity 'hot spot' associated with $\kappa \propto \delta(x - L/4)$ and located over the bathymetric constriction where squeezing is greatest — showing how positive correlations between κ and squeezing can dramatically increase the net tracer diffusivity κ_s.

3 Effect of squeeze dispersion on the circulation of oceanic tracers

In this section we show that squeeze dispersion affects the diapycnal diffusion of tracers on the scales of ocean circulation in continuous, depth-dependent stratification and flow. For this we use a series of two averages introduced by both De Szoeke and Bennett (1993) and Young (2012) to obtain a description of circulation-scale oceanic tracers that distinguishes between advection by the residual-mean circulation, isopycnal dispersion by mesoscale eddies, and diapycnal squeeze dispersion by microstructure turbulence.

We first apply a spatial *microstructure average* over turbulent fluctuations and density inversions on scales of centimeters to 10 meters. The microstructure average *(i)* yields a monotonic density field and enables the use of buoyancy coordinates, and *(ii)* permits the turbulent closure $\overline{\tilde{\boldsymbol{u}} \tilde{c}} = -\kappa \nabla c$ for the average microstructure turbulent flux $\overline{\tilde{\boldsymbol{u}} \tilde{c}}$, where $\tilde{\boldsymbol{u}}$ is the microstructure velocity field, $\tilde{c}$ is the microstructure tracer concentration, κ is the microstructure turbulent diffusivity and ∇c is the 'macroscale' tracer gradient. The macroscale tracer concentration c then obeys

$$c_t + \boldsymbol{u} \cdot \nabla c = \nabla \cdot \left(\kappa \nabla c \right) , \tag{7}$$

where the advecting velocity field $\boldsymbol{u}$ includes large scale internal waves as well as submesoscale, quasi-geostrophic, and bathymetric flows with vertical scales larger than 10 meters.

We introduce a second, thickness-weighted 'macroscale average' defined for any variable ϕ via

$$\hat{\phi} \stackrel{\text{def}}{=} \frac{\langle h \phi \rangle}{\langle h \rangle} \, . \tag{8}$$

In (8), $h \stackrel{\text{def}}{=} g / b_z$ is the 'thickness' of the buoyancy surface $b = -g \rho' / \rho_0$, where g is gravitational acceleration, ρ_0 is a reference potential density, and ρ' is the potential density perturbation therefrom. The angle brackets in (8) denote an ensemble, time, or spatial average over macroscale fluctuations in buoyancy coordinates (Young, 2012). Though our results are strictly true only for ensemble averages, time or spatial averages may be used where ensembles of oceanic motion are not available (Davis, 1994). Averaging in buoyancy coordinates is crucial for distinguishing between fundamental circulation processes: advection of tracer by the residual velocity, stirring of tracers along mean isopycnal surfaces by mesoscale eddies, and mixing across mean density surfaces by microstructure turbulence.

We show in appendix B that applying the thickness-weighted average in (8) to the macroscale tracer equation (7) leads to an equation for the evolution of tracers on the scales of ocean circulation:

$$\Big(\partial_t + \boldsymbol{u}^{\#} \cdot \nabla - \partial_z \underbrace{\langle h \rangle \left\langle \frac{\kappa}{h} \right\rangle}_{\stackrel{\text{def}}{=} \kappa_s} \partial_z \Big) \hat{c} = -\nabla \cdot \boldsymbol{E}^c \,. \tag{9}$$

Equation (9) describes the dispersion of the large-scale tracer concentration $\hat{c}$ due to advection by the circulation velocity $\boldsymbol{u}^{\#}$, stirring and diffusion by macroscale eddy fluxes $\boldsymbol{E}^c$ defined in (B.14), and across-isopycnal diffusion due to the effective diapycnal diffusivity $\kappa_s = \langle h \rangle \langle \kappa / h \rangle$.

In ocean models that do not resolve mesoscale eddies, the velocity field $\boldsymbol{u}^{\#}$ corresponds to the sum of the modeled velocity field and a 'bolus' velocity parameterized by the Gent-McWilliams scheme (Gent & Mcwilliams, 1990), while the isopycnal components of the eddy fluxes $\boldsymbol{E}^c$ are parameterized by the Redi diffusivity (Redi, 1982). These two terms dominate the isopycnal dispersion of oceanic tracers at large scales. Equation (9) demonstrates how diapycnal squeeze dispersion joins these isopycnal terms to determine the total dispersion of oceanic tracers.

The effective diapycnal diffusivity experienced by oceanic tracers is given by the squeeze dispersion formula $\kappa_s = \langle h \rangle \langle \kappa / h \rangle$, directly analogous to the effective diffusivity (6) that emerges in the parameterization in the introduction and the barotropic problem in section 2. The discretized argument developed in the introduction thus translates to cases with continuous stratification and flow, in which advection by vertically convergent and divergent flows acts to increase and decrease vertical tracer gradients. The mediation of oceanic tracer diffusion by squeeze dispersion implies an outsized importance for correlations — either dynamical or coincidental — between squeezing and microstructure turbulence.

4 Squeeze dispersion in the Samoan Passage

To demonstrate the importance of squeeze dispersion in observed oceanic scenarios, we evaluate the effect of squeeze dispersion on a hypothetical tracer advected along isopycnals in observations of abyssal flow through the Samoan Passage, a 40 km-wide deep conduit between the northern and southern Pacific Ocean. The configuration of strong abyssal Samoan Passage flow over rough and constricted bathymetry produces hydraulic jumps, lee waves, and strong diapycnal turbulence in addition to flow acceleration and squeezing. We focus on the flow through the eastern channel of the Samoan Passage using a series of hydrographic and direct turbulence observations made in 2012 summarized in figure 3(a) and by Alford et al. (2013).

Our analysis uses 18 Sea-Bird 911plus Conductivity-Temperature-Depth (CTD) profiles and 13 profiles by a Rockland Vertical Microstructure Profiler (VMP) that measured fluctuations in small-scale shear, temperature, and depth. Because conductivity was not measured by the VMP, we estimate VMP salinity with a 5th-order polynomial fit to the temperature-salinity relationship measured by nearby CTD profiles. The local turbulent kinetic energy dissipation rate, ϵ, is estimated from the VMP data by fitting local shear fluctuation spectra to the Nasmyth spectrum (Oakey & Elliott, 1982) and further integrating following Gregg (1998). We then estimate turbulent diffusivity via $\kappa = \Gamma \epsilon / N^2$, where N is the local buoyancy frequency and $\Gamma = 0.2$ is the mixing coefficient (Osborn, 1980). Density profiles at depth from both instruments are shown in figure 3(b).

To interpret the turbulence observations along deep Samoan Passage isopycnals, we define 21 density layers between $45.86 < \rho < 45.96\,\mathrm{kg/m^3}$ with width $\Delta\rho = 0.005\,\mathrm{kg/m^3}$, where ρ is potential density referenced to 4,000 meters. The density profiles from the CTD

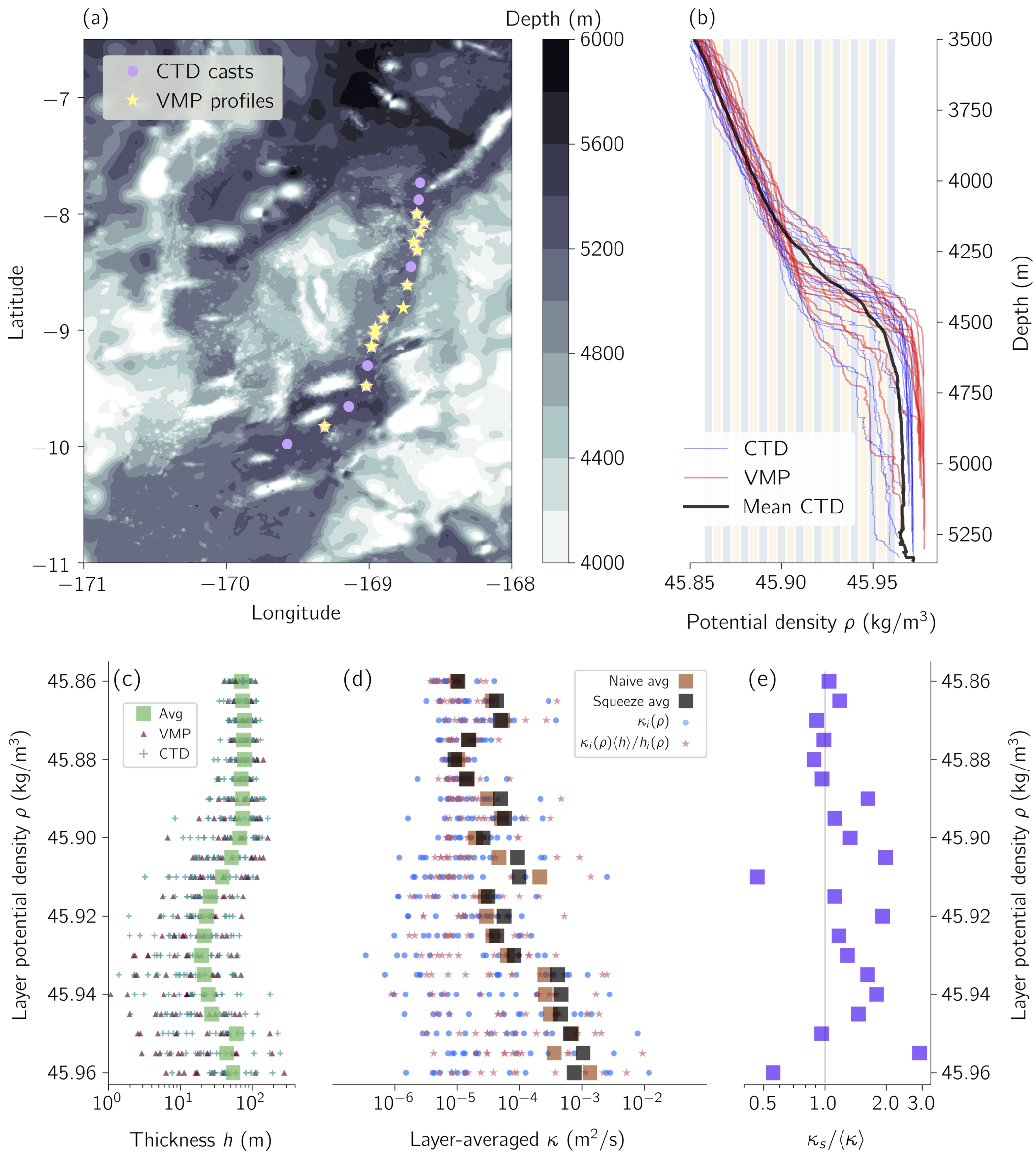

Figure 3: Effect of squeezing on diapycnal dispersion in the Samoan passage. (a) is a map of Samoan Passage bathymetry with CTD casts and VMP profiles used in (b–e). (b) shows CTD density profiles in blue, VMP density profiles in red, the mean CTD density profile in black and stripes to identify the 21 density layers used in analysis. (c), (d), and (e) show the layer-wise isopycnal thickness $h(\rho)$, diffusivity κ, and diffusivity enhancement $\kappa_s/\langle\kappa\rangle$ due to squeeze dispersion. Positive correlations between squeezing and turbulence imply that $\kappa_s/\langle\kappa\rangle$ is greater than 1, while negative correlations imply $\kappa_s/\langle\kappa\rangle$ is less than 1.

and VMP profiles are shown in figure 3(b) overlain by stripes that indicate the density layers. The thickness of each density layer defined by $h(\rho) = z\,(\rho - \Delta\rho/2) - z\,(\rho + \Delta\rho/2)$ are plotted in figure 3(b) and range from ~14–104 meters.

We define a spatial 'passage average' as an average over the VMP and CTD profiles for density, and the VMP profiles for turbulent diffusivity κ, so that the average of a variable ϕ is

$$\langle \phi \rangle (\rho) = \frac{1}{n} \sum_{i}^{n} \phi_i(\rho) \, , \tag{10}$$

where ρ is the central density in the density layer and n is the number of profiles used in the average. For averages of density or thickness $n = 31$ and includes both the CTD and VMP profiles, while averages of turbulent diffusivity use only the VMP profiles so that $n = 13$.

We then compare the effective squeeze diffusivity $\kappa_s = \langle h \rangle \langle \kappa/h \rangle$ with the average diffusivity $\langle \kappa \rangle$ across each density layer. Figure 3(d) plots the result along with the layer-averaged diffusivities for each profile, $\kappa_i(\rho)$, and the scaled diffusivities $\langle h \rangle \kappa_i/h_i$ that form the kernel of the squeeze-average. Figure 3(e) plots the ratio between the average and effective diffusivities. On some isopycnals, the effective diffusivity κ_s is smaller than $\langle \kappa \rangle$ due to negative correlations between isopycnal squeezing and turbulent diffusivity. However, most isopycnals in the abyssal Samoan Passage experience an effective diffusivity κ_s that is larger — up to 3 times larger — than the average diffusivity $\langle \kappa \rangle$ due to positive correlations between squeezing and turbulence. This diffusivity enhancement is most prominent on deep isopycnals on which κ is large, and thus where mixing matters most.

Voet et al. (2015) compared heat budget-based mixing estimates to in-situ estimates of turbulent mixing, finding that the budget-based estimates are 2 to 6 times larger than naively region-averaged in-situ observations. While undersampling of mixing hot-spots could produce this mismatch, our results suggest that squeeze dispersion also plays a role.

5 Conclusions

'Squeeze dispersion' is a kinematic process that modulates and enhances oceanic diapycnal mixing when isopycnal surfaces are squeezed together and stretched apart by fluctuating flow. The importance of squeeze dispersion depends on *(i)* the magnitude of oceanic vertical strain and squeezing and *(ii)* correlations between squeezing and diapycnal turbulent mixing. Squeezing is often weak in mesoscale oceanic flows, being proportional to Rossby number in quasi-geostrophic flows or the nonlinearity of internal wave fields. Yet plausible dynamical mechanisms may link mixing and strain: for example, squeezing and intense turbulent mixing are co-located over mountainous bathymetry in the Samoan Passage. Numerical simulations suggest that large-scale strain may enhance turbulent intensity and mixing in preexisting shear layers (Kaminski, 2016). On the other hand, Alford and Pinkel (2000) find a *negative* correlation between squeezing and turbulent overturns and mixing in the near-surface ocean. Further observations and simulations are needed to determine the relationship between oceanic strain and turbulent mixing throughout the water column, especially where turbulence is strong and κ is large.

Connecting microstructure turbulence to oceanic tracer dispersion in the presence of squeeze dispersion requires context. Consider the parameterization $\kappa = \Gamma\epsilon/N^2$ for turbulent diffusivity κ in terms of turbulent kinetic energy dissipation rate ϵ, buoyancy frequency N^2, and mixing coefficient Γ. Noting that the isopycnal thickness in equation (1) is $h = g/b_z = g/N^2$, equation (1) implies that the effective diffusivity associated with repeated measurements of ϵ and N^2 on an isopycnal b is

$$\kappa_s = \frac{\langle \Gamma \epsilon \rangle}{\langle N^2 \rangle} \,, \tag{11}$$

where the brackets denote an average on the isopycnal b over macroscale fluctuations. κ_s in (11) is then the effective diffusivity acting on large-scale oceanic tracers at the average depth of the surface b. Equation (11) differs from the average diapycnal diffusivity $\kappa = \left\langle \Gamma \epsilon / N^2 \right\rangle$ especially when ϵ and N^2 are negatively correlated — that is, when turbulent dissipation and squeezing are positively correlated.

Squeeze dispersion is not shear dispersion. For example, vertical oceanic shear dispersion is associated with lateral variations in vertical velocity and has an effect that is inversely proportional to lateral diffusivity. Vertical squeeze dispersion, on the other hand, persists under vanishing lateral diffusivity and is proportional to the strength of the vertical diffusivity.

The effective diffusivity for large-scale tracers in equation (1) implies that models that use the local average diffusivity but do not fully resolve oceanic strain may underpredict oceanic tracer dispersion. In other words, the effective diffusivities in coarse resolution models should take unresolved squeezing into account. Finally, squeeze dispersion may also be important in other, non-oceanic laminar flows such as confined low Reynolds number flows. In these cases, the thickness h that appears in equation (1) should be interpreted as the separation between material surfaces.

A Barotropic advection of tracer over bathymetry

Introducing the topographic coordinate $\tilde{z} = z \langle H \rangle / H$, where $\langle H \rangle$ is a constant average depth and $\langle \phi \rangle = L^{-1} \int_0^L \phi \, \mathrm{d}x$ is the average of any quantity ϕ over a tracer trajectory from $x = 0$ to $x = L$, the tracer conservation equation (2) with flow field (3) transforms into

$$c_t + u c_x = \frac{\langle H \rangle^2 \kappa}{H^2} c_{\tilde{z}\tilde{z}} \,. \tag{A.1}$$

In a coordinate frame following columns of fluid advected horizontally by the flow $u = U/H$ with transport U, the vertical spread of the tracer is described by the deceptively ordinary equation

$$c_s = \langle \kappa \rangle \, c_{\tilde{z}\tilde{z}} \,, \tag{A.2}$$

where $\langle \kappa \rangle$ denotes the average values of κ over a trajectory. In (A.2), s is a time-like trajectory coordinate defined by

$$s(t) \stackrel{\text{def}}{=} \frac{\langle H \rangle^2}{\langle \kappa \rangle \, U} \int_{t_i}^{t} \frac{\kappa}{H} \, \mathrm{d}t' \,, \tag{A.3}$$

where $\kappa(x, t)$ and $H(x)$ are evaluated along the column trajectory $x = \xi(t)$, which obeys $\xi_t = u(\xi)$. The solution to (A.2) on short trajectories and with the initial condition $c = \delta(\tilde{z} - \tilde{z}_0)\delta(x - x_0)$ is

$$c = \frac{1}{\sqrt{4\pi \langle \kappa \rangle s}} \exp\left[-\frac{(\tilde{z} - \tilde{z}_0)^2}{4 \langle \kappa \rangle s} \right] \delta(x - \xi) \,. \tag{A.4}$$

The solution (A.4) is valid when the tracer concentration is negligible at the boundaries, which holds if the trajectory is short and the initial release point $\tilde{z}_0$ is sufficiently far from the top or bottom. Evaluating (A.4) at $t = \langle H \rangle L / U$ when the tracer patch reaches $x = L$ yields equation (5).

B Derivation of the tracer circulation equation (9)

To derive the tracer circulation equation (9), we apply the thickness-weighted average defined in (8) to the macroscale tracer equation,

$$c_t + \boldsymbol{u} \cdot \nabla c = \nabla \cdot (\kappa \nabla c) \ , \tag{B.1}$$

first introduced in equation (7). We introduce the variable $\varsigma \stackrel{\text{def}}{=} 1/b_z$ in this appendix for convenience. ς is related to the thickness $h = g/b_z$ via $\varsigma = h/g$ and corresponds to the variable σ in Young (2012). In terms of ς the thickness-weighted average in (8) is $\hat{\phi} \stackrel{\text{def}}{=} \langle \varsigma\phi \rangle \,/\, \langle \varsigma \rangle$ for any variable ϕ.

We first transform the macroscale tracer equation (B.1) from the Cartesian coordinates x, y, z, t to the buoyancy coordinates $\tilde{x}, \tilde{y}, \tilde{b}, \tilde{t}$. A thorough review of buoyancy coordinates is given in Young (2012). The material derivative $\mathrm{D}/\mathrm{D}t \stackrel{\text{def}}{=} \boldsymbol{u} \cdot \nabla c = u\partial_x + v\partial_y + w\partial_z$ in buoyancy coordinates is

$$\frac{\mathrm{D}}{\mathrm{D}t} = u\partial_{\tilde{x}} + v\partial_{\tilde{y}} + \varpi\partial_{\tilde{b}} \, , \tag{B.2}$$

where ϖ is the diabatic contribution to the buoyancy conservation equation such that $\mathrm{D}b/\mathrm{D}t = \varpi$. We define ϖ as

$$\varpi \stackrel{\text{def}}{=} \nabla \cdot (\kappa \nabla b) \ , \tag{B.3}$$

consistent with the diabatic contribution to the macroscale tracer equation (B.1). In other words, we use a closure with turbulent diffusivity κ to approximate the effect of mictrostructure fluxes for all tracers.

We simplify the microscale diabatic term $\nabla\cdot(\kappa\nabla c)$ on the right side of (B.1) with two assumptions. First, we assume that buoyancy surfaces have small slopes and neglect terms proportional to $\zeta_{\tilde{x}}$ or $\zeta_{\tilde{y}}$, where $z = \zeta(\tilde{x}, \tilde{y}, \tilde{b}, \tilde{t})$ is the height of the buoyancy surface $\tilde{b}$. Second, we assume diffusive isopycnal tracer fluxes on circulation scales are dominated by macroscale stirring rather than microscale turbulence. We thus consider only the diabatic component of the diabatic flux, so that

$$\kappa \nabla c \approx \frac{\kappa c_{\tilde{b}}}{\varsigma^2} \mathbf{e}_3 \, , \tag{B.4}$$

where $\mathbf{e}_3 = \mathbf{k}/\varsigma$ is the third covariant buoyancy-coordinate basis vector (Young, 2012) and $\mathbf{i}$, $\mathbf{j}$, and $\mathbf{k}$ are the east, north, and vertical Cartesian coordinate unit vectors. Applying the same assumptions to the diabatic buoyancy flux implies that $\varpi \approx \varsigma^{-1}\partial_{\tilde{b}}\,(\kappa/\varsigma)$.

We turn to the thickness-weighted average of the advection term $\mathrm{D}c/\mathrm{D}t$ in (B.1). For any variable ϕ, the thickness-weighted decomposition

$$\phi = \hat{\phi} + \phi'' \tag{B.5}$$

defines the perturbation ϕ''. A key identity derived by Young (2012) is

$$\left\langle \varsigma \frac{\mathrm{D}c}{\mathrm{D}t} \right\rangle = \langle \varsigma \rangle \left(\frac{\mathrm{D}^{\#}\hat{c}}{\mathrm{D}t} + \nabla \cdot \boldsymbol{J}^c \right) , \tag{B.6}$$

where the residual material derivative

$$\frac{\mathrm{D}^{\#}}{\mathrm{D}t} \stackrel{\text{def}}{=} \hat{u}\partial_x + \hat{v}\partial_y + w^{\#}\partial_z \tag{B.7}$$

describes advection by the residual velocity field $\boldsymbol{u}^{\#} = (\hat{u}, \hat{v}, w^{\#})$. The meaning of $w^{\#}$ is described in the next paragraph. The perturbation flux in (B.6) is

$$\boldsymbol{J}^c \stackrel{\text{def}}{=} \widehat{u''c''}\,\langle \mathbf{e}_1 \rangle + \widehat{v''c''}\,\langle \mathbf{e}_2 \rangle + \widehat{\varpi''c''}\,\langle \mathbf{e}_3 \rangle \tag{B.8}$$

where the average basis vectors $\langle \mathbf{e}_j \rangle$ are defined

$$\langle \mathbf{e}_1 \rangle \stackrel{\text{def}}{=} \mathbf{i} - \mathbf{k} b_x^{\#} / b_z^{\#} \, , \quad \langle \mathbf{e}_2 \rangle \stackrel{\text{def}}{=} \mathbf{j} - \mathbf{k} b_y^{\#} / b_z^{\#} \, , \quad \langle \mathbf{e}_3 \rangle \stackrel{\text{def}}{=} \mathbf{k} / b_z^{\#} \, . \tag{B.9}$$

The vertical velocity $w^{\#}$ in (B.7) and buoyancy field $b^{\#}$ in (B.9) are defined in terms of the average depth of a buoyancy surface, $\langle \zeta \rangle$. In particular, $b^{\#}$ is defined via $z = \langle \zeta \rangle (\tilde{x}, \tilde{y}, b^{\#}, \tilde{t})$ and is therefore the value of the buoyancy surface whose mean position is $\boldsymbol{x}, t$. The residual vertical velocity $w^{\#}$, on the other hand, is defined in terms of the motion of $\langle \zeta \rangle$ via

$$w^{\#} \stackrel{\text{def}}{=} \frac{\mathrm{D}^{\#} \langle \zeta \rangle}{\mathrm{D} t} \, . \tag{B.10}$$

In this sense, $w^{\#}$ and $\langle \zeta \rangle$ have a similar relationship as w and ζ. Neither $w^{\#}$ nor $b^{\#}$ are equal to their thickness-weighted counterparts $\hat{w}$ and $\hat{b}$.

Turning back to the diabatic contribution on the right of (B.1), we use (B.4) and the identity $\langle \varsigma \nabla \cdot \boldsymbol{F} \rangle = \nabla \cdot \hat{F}^j \langle \mathbf{e}_j \rangle$ to obtain

$$\widehat{\nabla \cdot (\kappa \nabla c)} = \nabla \cdot \frac{\langle \kappa / \varsigma \rangle \, \hat{c}_{\tilde{b}} + \left\langle \kappa c''_{\tilde{b}} / \varsigma \right\rangle}{\langle \varsigma \rangle} \langle \mathbf{e}_3 \rangle \, . \tag{B.11}$$

We then use $\varpi = \varsigma^{-1} \partial_{\tilde{b}} (\kappa / \varsigma)$ to combine (B.11) with the divergence of the diapycnal term $\widehat{\varpi'' c''} \langle \mathbf{e}_3 \rangle$ in (B.8) and transform the part of the result that depends on $\hat{c}$ to Cartesian coordinates. When the dust settles, we find that

$$\nabla \cdot \widehat{(\varpi'' c'' - \kappa \nabla c)} \langle \mathbf{e}_3 \rangle = - \partial_z \left(\langle \varsigma \rangle \left\langle \frac{\kappa}{\varsigma} \right\rangle \partial_z \right) \hat{c} + \nabla \cdot \frac{\left\langle c'' \partial_{\tilde{b}} (\kappa / \varsigma) - \kappa c''_{\tilde{b}} / \varsigma \right\rangle}{\langle \varsigma \rangle} \langle \mathbf{e}_3 \rangle \, . \tag{B.12}$$

The first term on the right of (B.12) describes the squeeze dispersion of $\hat{c}$, while the second term corresponds to the diabatic macroscale perturbation flux associated with the difference between the tracer distribution c and buoyancy distribution b.

We use (B.6) and (B.12) to write the thickness-weighted-average of (7):

$$\left(\partial_t + \boldsymbol{u}^{\#} \cdot \nabla - \partial_z \kappa_s \partial_z \right) \hat{c} = - \nabla \cdot \boldsymbol{E}^c \, , \tag{B.13}$$

where $\kappa_s \stackrel{\text{def}}{=} \langle h \rangle \langle \kappa / h \rangle = \langle \varsigma \rangle \langle \kappa / \varsigma \rangle$ and

$$\boldsymbol{E}^c \stackrel{\text{def}}{=} \widehat{u'' c''} \langle \mathbf{e}_1 \rangle + \widehat{v'' c''} \langle \mathbf{e}_2 \rangle + \langle \varsigma \rangle^{-1} \left\langle c'' \partial_{\tilde{b}} (\kappa / \varsigma) - \kappa c''_{\tilde{b}} / \varsigma \right\rangle \langle \mathbf{e}_3 \rangle \, . \tag{B.14}$$

Acknowledgments

GLW was supported by the NOAA Climate and Global Change Postdoctoral Fellowship Program, administered by UCAR's Cooperative Programs for the Advancement of Earth System Sciences. Samoan Passage research was funded by the National Science Foundation under grants OCE-1029268, OCE-1029483 and OCE-1657795. Julia code and notebooks to generate figures 2 and 3 can be found at `https://github.com/glwagner/SqueezeDispersionGRL`.

References

Alford, M. H., Girton, J. B., Voet, G., Carter, G. S., Mickett, J. B., & Klymak, J. M. (2013). Turbulent mixing and hydraulic control of abyssal water in the Samoan Passage. *Geophysical Research Letters*, *40*(17), 4668–4674.

Alford, M. H., & Pinkel, R. (2000). Observations of overturning in the thermocline: The context of ocean mixing. *Journal of Physical Oceanography*, *30*(5), 805–832.

Aris, R. (1956). On the dispersion of a solute in a fluid flowing through a tube. *Proc. R. Soc. Lond. A*, *235*(1200), 67–77.

Davis, R. E. (1994). Diapycnal mixing in the ocean: Equations for large-scale budgets. *Journal of physical oceanography*, *24*(4), 777–800.

De Szoeke, R. A., & Bennett, A. F. (1993). Microstructure fluxes across density surfaces. *Journal of physical oceanography*, *23*(10), 2254–2264.

Gent, P. R., & Mcwilliams, J. C. (1990). Isopycnal mixing in ocean circulation models. *Journal of Physical Oceanography*, *20*(1), 150–155.

Gregg, M. (1998). Estimation and geography of diapycnal mixing in the stratified ocean. *Physical processes in lakes and oceans*, 305–338.

Kaminski, A. K. (2016). *Linear optimal perturbations and transition to turbulence in strongly-stratified shear flows* (Unpublished doctoral dissertation). University of Cambridge.

Ledwell, J., Montgomery, E., Polzin, K., Laurent, L. S., Schmitt, R., & Toole, J. (2000). Evidence for enhanced mixing over rough topography in the abyssal ocean. *Nature*, *403*(6766), 179.

Ledwell, J., St. Laurent, L., Girton, J., & Toole, J. (2011). Diapycnal mixing in the Antarctic circumpolar current. *Journal of Physical Oceanography*, *41*(1), 241–246.

Mashayek, A., Ferrari, R., Merrifield, S., Ledwell, J. R., St Laurent, L., & Garabato, A. N. (2017). Topographic enhancement of vertical turbulent mixing in the Southern Ocean. *Nature Communications*, *8*, 14197.

Oakey, N., & Elliott, J. (1982). Dissipation within the surface mixed layer. *Journal of Physical Oceanography*, *12*(2), 171–185.

Osborn, T. (1980). Estimates of the local rate of vertical diffusion from dissipation measurements. *Journal of Physical Oceanography*, *10*(1), 83–89.

Redi, M. H. (1982). Oceanic isopycnal mixing by coordinate rotation. *Journal of Physical Oceanography*, *12*(10), 1154–1158.

St. Laurent, L., Naveira Garabato, A. C., Ledwell, J. R., Thurnherr, A. M., Toole, J. M., & Watson, A. J. (2012). Turbulence and diapycnal mixing in Drake Passage. *Journal of Physical Oceanography*, *42*(12), 2143–2152.

Voet, G., Girton, J. B., Alford, M. H., Carter, G. S., Klymak, J. M., & Mickett, J. B. (2015). Pathways, volume transport, and mixing of abyssal water in the Samoan Passage. *Journal of Physical Oceanography*, *45*(2), 562–588.

Watson, A. J., Ledwell, J. R., Messias, M.-J., King, B. A., Mackay, N., Meredith, M. P., ... Garabato, A. C. N. (2013). Rapid cross-density ocean mixing at mid-depths in the Drake Passage measured by tracer release. *Nature*, *501*(7467), 408.

Young, W. R. (2012). An exact thickness-weighted average formulation of the Boussinesq equations. *Journal of Physical Oceanography*, *42*(5), 692–707.